Measurement of Through-Going Particle Momentum By Means Of Multiple Scattering With The ICARUS T600 TPC

A. Ankowski [a], M. Antonello [b], P. Aprili [c], F. Arneodo [c], A. Badertscher [d], B. Baiboussinov [e], M. Baldo Ceolin [e], G. Battistoni [f], P. Benetti [g], A. Borio di Tigliole [g], R. Brunetti [g, 1], A. Bueno [h,*], E. Calligarich [g], F. Carbonara [i], M.C. Carmona [h], F. Cavanna [b], P. Cennini [j], S. Centro [e], A. Cesana [k], D.B. Cline [ℓ], K. Cieślik [m], A.G. Cocco [i], C. De Vecchi [g], A. Dąbrowska [m], A. Di Cicco [i], R. Dolfini [g], A. Ereditato [i], A. Ferrari [j], G. Fiorillo [i], D. García-Gamez [h], Y. Ge [d], D. Gibin [e], A. Gigli Berzolari [g], I. Gil-Botella [n], K. Graczyk [a], L. Grandi [g], A. Guglielmi [e], J. Holeczek [o], D. Kiełczewska [p] J. Kisiel [o], T. Kozłowski [q], M. Laffranchi [d], J. Łagoda [p], B. Lisowski [ℓ], J. Lozano [h], M. Markiewicz [m], A. Martínez de la Ossa [h], C. Matthey [ℓ], F. Mauri [g], A.J. Melgarejo [h], A. Menegolli [g], G. Meng [e], M. Messina [d], P. Mijakowski [q], C. Montanari [g], S. Muraro [f], S. Navas-Concha [h], J. Nowak [a], S. Otwinowski [ℓ], O. Palamara [c], L. Periale [r], G. Piano Mortari [b], A. Piazzoli [g], P. Picchi [r], F. Pietropaolo [e], W. Półchłopek [s], M. Posiadała [p], M. Prata [g], M.C. Prata [g], P. Przewlocki [q], A. Rappoldi [g], G.L Raselli [g], E. Rondio [q], M. Rossella [g], B. Rossi [i], A. Rubbia [d], C. Rubbia [g], P.R. Sala [f], D. Scannicchio [g], E. Segreto [b], Y. Seo [ℓ], F. Sergiampietri [t], J. Sobczyk [a], D. Stefan [m], J. Stepaniak [q], R. Sulej [u], M. Szeptycka [q], M. Szarska [m], M. Terrani [k], F. Varanini [e], S. Ventura [e], C. Vignoli [g], T. Wąchała [m], H. Wang [ℓ], X. Yang [ℓ], A. Zalewska [m]

[a] *Institute of Theoretical Physics, Wrocław University, Wrocław, Poland*

[b] *Gruppo collegato INFN and Dipartimento di Fisica, Università dell'Aquila, L'Aquila, Italy*

[c] *Laboratori Nazionali del Gran Sasso (LNGS) INFN, Assergi, Italy*

[d] *Institute for Particle Physics, ETH Hönggerberg, Zürich, Switzerland*

[e] *Dipartimento di Fisica, Università di Padova and INFN, Padova, Italy*

[f] *Dipartimento di Fisica, Università di Milano and INFN, Milano, Italy*

[g] *Dipartimento di Fisica Nucleare e Teorica, Università di Pavia and INFN, via Bassi 6, I-27100 Pavia, Italy*

[h] *Departamento de Física Teórica y del Cosmos and Centro Andaluz de Física de Partículas Elementales (CAFPE), Universidad de Granada, Granada, Spain*

[i] *Dipartimento di Scienze Fisiche , Università Federico II di Napoli and INFN, Napoli, Italy*

[j] *CERN, Genève, Switzerland*

[1] Present address: INFN, Torino, Italy.

[k] *Dipartimento di Ingegneria Nucleare, Politecnico di Milano and INFN, Milano, Italy*
[ℓ] *Department of Physics and Astronomy, University of California, Los Angeles, USA*
[m] *H. Niewodniczański Institute of Nuclear Physics, Kraków, Poland*
[n] *CIEMAT, Departamento de Investigacion Basica, Madrid, Spain*
[o] *Institute of Physics, University of Silesia, Katowice, Poland*
[p] *Institute of Experimental Physics, University of Warszawa, Poland*
[q] *A.Sołtan Institute for Nuclear Studies, Warszawa, Poland*
[r] *Laboratori Nazionali di Frascati (LNF) INFN, Frascati, Italy*
[s] *Department of Electronics, AGH University of Science and Technology, Kraków, Poland*
[t] *INFN, Pisa, Italy*
[u] *Institute of Radioelectronics, University of Warsaw, Warszawa, Poland*

Abstract

The ICARUS collaboration has demonstrated, following the operation of a 600 ton (T600) detector at shallow depth, that the technique based on liquid Argon TPCs is now mature. The study of rare events, not contemplated in the Standard Model, can greatly benefit from the use of this kind of detectors. In particular, a deeper understanding of atmospheric neutrino properties will be obtained thanks to the unprecedented quality of the data ICARUS provides. However if we concentrate on the T600 performance, most of the ν_μ charged current sample will be partially contained, due to the reduced dimensions of the detector. In this article, we address the problem of how well we can determine the kinematics of events having partially contained tracks. The analysis of a large sample of atmospheric muons collected during the T600 test run demonstrate that, in case the recorded track is at least one meter long, the muon momentum can be reconstructed by an algorithm that measures the Multiple Coulomb Scattering along the particle's path. Moreover, we show that momentum resolution can be improved by a factor two using an algorithm based on the Kalman Filtering technique.

Key words: Neutrino Detector, Liquid Argon, TPC, Multiple Scattering, Kalman Filter
PACS: 29.40.Gx, 29.85+c

* Corresponding author. Tel: +34-958-244152; fax.: +34-958-248529.
E-mail address: a.bueno@ugr.es.

1 Introduction

Liquid Argon TPCs are a most promising technique for the study of several fundamental topics of particle physics: neutrino properties, proton decay and dark matter. After an extensive R&D programme, the ICARUS collaboration was able to operate at shallow depth a detector of 600 tons (T600) [1]. The successful completion of a series of technical tests has shown that the liquid Argon technique is now mature. The sample of cosmic ray events recorded have provided us with a statistically significant data set of unprecedented quality. Long muon tracks, stopping muons, muon bundles, hadronic and electromagnetic showers as well as low energy events have been studied and results have been published elsewhere [2,3,4,5,6].

The T600 detector is now at the INFN Gran Sasso Laboratory. It is being installed to be operated underground. Its physics programme has been reviewed in [7]. Among the different non-accelerator physics topics that can be covered with such a detector, the study of atmospheric neutrinos is particularly important. Thanks to its high granularity, ICARUS can separate, for all neutrino species, charged current and neutral current events down to production thresholds and free of detector biases. Therefore it provides a data set of very high quality (specially in the sub GeV region) and almost free of systematic uncertainties (which are nowadays the limiting factor in the study of atmospheric neutrino oscillations).

Atmospheric ν_μ charged current interactions will produce prompt muons with mean energy of several hundreds of MeV. They will have travel paths of several meters, since minimum ionizing particles deposit about 210 MeV per meter in Argon. However due to the reduced transverse dimensions of the T600 detector, a large fraction of the recorded ν_μ charged current will be partially contained. Calorimetric measurements will be highly inadequate to study this sort of events. To extract valuable kinematic information from them, we can take advantage of the multiple Coulomb scattering underwent by muons as they propagate through liquid Argon. Momentum measurement of partially contained tracks will be performed in a way much similar to the one used in emulsion experiments. Together with this method, we try to apply a new technique, known as Kalman Filter [8], in oder to obtain a more precise measurement of the particle momenta.

This article is organized as follows: Section 2 gives a brief outline of the detector. In Section 3 we discuss the technical aspects of the Monte-Carlo simulation and event reconstruction. Section 4 describes what we called the *classical* approach to momentum measurement by means of multiple Coulomb scattering. In Sections 5 and 6 we briefly introduce the Kalman Filter technique and how it can be used to obtain an estimation of momenta for through-going particles. Section 7 compares the performance of the two algorithms. To evaluate the goodness of the Kalman Filter method, Section 8 describes the results obtained when the Kalman Filter algorithm is applied to real data: in our

case, a sample of atmospheric stopping muons. Conclusions are finally drawn in Section 9.

2 The 600 Ton Liquid Argon TPC

The ICARUS T600 liquid Argon (LAr) detector [1] consists of a large cryostat split in two identical, adjacent half-modules, with internal dimensions $3.6 \times 3.9 \times 19.6$ m^3 each of them. Each half-module is an independent unit housing an internal detector composed by two Time Projection Chambers (TPC), a field shaping system, monitors, probes, and two arrays of photo-multipliers. Externally the cryostat is surrounded by a set of thermal insulation layers. The TPC wire read-out electronics is located on the top side of the cryostat. The detector layout is completed by a cryogenic plant made of a liquid Nitrogen cooling circuit to maintain uniform the LAr temperature, and of a system of LAr purifiers.

A liquid Argon TPC detects the ionization charge released at the passage of charged particles in the volume of LAr, thus providing three dimensional image reconstruction and calorimetric measurement of ionizing events. The detector, equipped with an electronic read-out system, works as an "electronic bubble chamber" employing LAr as ionization medium.

An uniform electric field applied to the medium makes the ionization electrons drift onto the anode; thanks to the low transverse diffusion of the ionization charge, the electron images of ionizing tracks are preserved. Successive anode wire planes, biased at a different potential and oriented at different angles, make possible the three dimensional reconstruction of the track image.

In each T600 half-module, the two identical TPCs are separated by a common cathode. Each TPC consists of three parallel wire planes: the first, facing the drift region, with horizontal wires (Induction plane); the other two with the wires at $\pm 60^0$ from the horizontal direction (Induction and Collection planes, respectively). The wire pitch is 3 mm. The maximum drift path (distance between the cathode and the wire planes) is 1.5 m and the nominal drift field 500 V/cm. The measured drift velocity is 1.55 ± 0.02 mm/μs [3].

Each wire of the chamber is independently digitized every 400 ns. The electronics was designed to allow continuous read-out, digitization and independent waveform recording of signals from each wire of the TPC. Measurement of the time when the ionizing event occurred (so called "t_0 time" of the event), together with the electron drift velocity information, provides the absolute position of the tracks along the drift coordinate. The t_0 can be determined by detection of the prompt scintillation light produced by ionizing particles in LAr [9].

3 Monte-Carlo simulation and event reconstruction

Our goal is to understand how accurately we can measure the momentum of charged particles that traverse the T600 detector without stopping. To this purpose, we have carried out a full simulation of muons that span a momentum range going from 250 MeV up to 6 GeV. This is the relevant energy range for the study of atmospheric neutrinos.

The FLUKA package [10] has been used to simulate all relevant physics processes (multiple Coulomb scattering, delta ray production, muon decay, energy loss by ionization, ...). The detector geometry has been simulated according to the detector description given in Section 2. Special care was put in reproducing the same experimental conditions met when the T600 test at shallow depth was carried out. Therefore we included a detailed simulation of the noise and of the electronic response of the detector.

The event reconstruction proceeded as follows: The wire output signals were used to identify hits (segment of track whose energy is recorded by a wire). Hits are fit in order to extract physical information (deposited charged, time and position). In a latter step, hits are grouped into clusters. From them, we reconstruct two dimensional tracks for each of the three wire planes (one collection and two induction views). Finally the spatial coordinates of the charged track (3D reconstruction) are obtained matching the hits of the 2D tracks previously reconstructed. The key point for 3D reconstruction is the fact that the drift coordinate is common to all three planes. This redundancy allows to associate hits from different planes to a common energy deposition. Finally 3D tracks are used to extract the information provided by multiple Coulomb scattering, and thus get a measurement of the track momentum. The same procedure was used to reconstruct the real data sample of stopping muons used in Section 8.

To exemplify how the reconstruction software works, figure 1 shows a view of a 0.5 GeV stopping muon(left panel) and its three-dimensional reconstruction (right panel).

4 The *classical* approach to momentum measurement

We discuss what hereafter will be referred to as the *classical* approach to momentum measurement. It profits from the fact that a charged particle traversing a medium is deflected through many small angle scatterings, θ_i. To estimate the momentum of a charged particle we use the following analytical

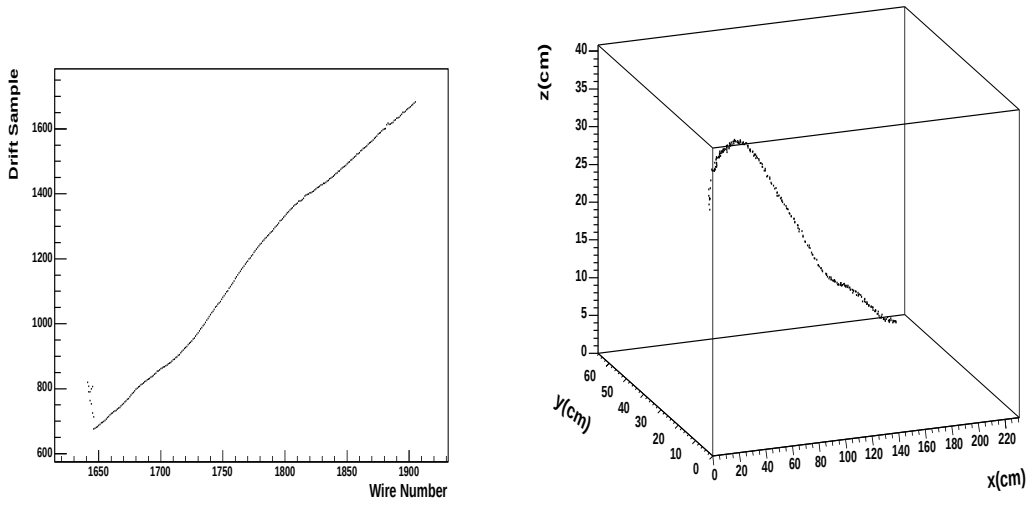

Fig. 1. Collection (2D) view of a typical stopping muon. 3D reconstruction of the same muon event (right).

expression [11]:

$$\theta_0^{rms} = \frac{13.6\ MeV}{\beta c\, p}\, z \sqrt{\frac{l}{X_0}} \left[1 + 0.038 \cdot ln\left(\frac{l}{X_0}\right)\right] \tag{1}$$

where θ_0^{rms} is the width of the Gaussian approximation used for the central 98% of the projected angular distribution. p, β and z are the momentum, velocity and charge of the incident particle. X_0 is the radiation length and l the considered segment length.

The procedure used to measure the momentum of the particle is as follows:

(1) The whole track is split into segments of a fixed length.
(2) For each segment, hits belonging to δ-rays are searched for and tagged, such that they can be excluded from the analysis. Otherwise delta ray hits can sensibly distort the determination of the segment direction.
(3) The remaining hits in each segment are fitted to a straight line, providing the segment direction.
(4) For each consecutive pair of segments, the scattering angle is calculated as the difference between their angles.
(5) We compute the RMS of the scattering angle distribution, after cutting out 2% of the tails (since only the 98% central interval of the Molière distribution is Gaussian).
(6) Finally to calculate the value of θ^{rms}, we consider all the angles but those whose distance to the mean is larger than 2.5 times the RMS value.

The measured RMS of the scattering angles distribution, θ_{meas}^{rms}, is related to

the "pure" Coulomb scattering θ_0^{rms} by the following expression:

$$(\theta_{meas}^{rms})^2 = (\theta_0^{rms})^2 + (\theta_{noise}^{rms})^2 \tag{2}$$

where θ_{noise}^{rms} is the angular detector resolution on the difference of two measured segment angles. In our case, it corresponds to the spatial resolution in the drift coordinate, σ, which is related to the error on the determination of each individual hit time. This magnitude was measured during the T600 run, using cosmic ray muons and test pulse data, to be about 400 μm. The noise contribution does not depend on the track momentum. It only depends on the segment length ($\theta_{noise}^{rms} \propto l_{seg}^{-3/2}$). Substituting in equation 2, we get:

$$\theta_{meas}^{rms} = \sqrt{(\theta_0^{rms})^2 \; + \; (\theta_{noise}^{rms})^2}$$

$$= \sqrt{\left(\frac{13.6 \; MeV}{\beta c \; p} \, z \sqrt{\frac{l}{X_0}} \cdot \left[1 + 0.038 \cdot ln\left(\frac{l}{X_0} \right) \right] \right)^2 \; + \; (C \cdot l^{-3/2})^2} \tag{3}$$

where C is just a proportionality constant for the noise.

To extract the track momentum, we measure θ_{meas}^{rms} for different segment lengths (l). A fit to those values, using equation 3, provides an estimation of p and C, which are taken as free parameters. This procedure allows to compute the momentum for each single track, since no other assumptions are made. In addition, with this original approach, we avoid the usual problem of choosing an optimal segment length for the determination of the momentum.

As an example, figure 2 shows the result obtained when this procedure is applied to a simulated 3 GeV muon. The triangles correspond to the experimentally measured RMS of the scattering angles for different values of the segment length. The curve indicates the fit result. The rising up at low values of l indicates the region where the contribution from detector resolution dominates, whereas at high values of l the main contribution comes from pure Coulomb scattering.

In this new approach, the key point to compute the momentum on a track by track basis is to decide the set of segment lengths that will be included in the fit. The minimum segment length should be such that effects due to multiple scattering emerge from detector noise. The optimal value for this minimum segment length is 5 cm. The maximum segment length should be short enough to allow as much entries as possible inside the angle distribution used to compute θ_{meas}^{rms}. This last value clearly depends on the recorded track length. To improve our results, we decided to split our sample into tracks having lengths longer than 2.5 meters and tracks shorter than 2.5 meters. In fact, this corresponds to a muon momentum cut at around 600 MeV. For long tracks we have used 13 segment lengths inside the interval [5 cm, 35 cm]. For

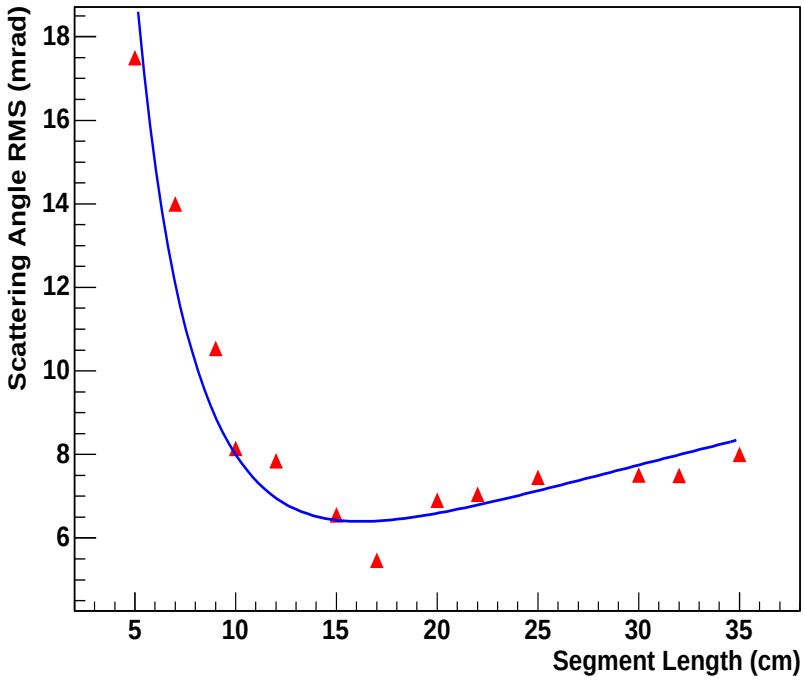

Fig. 2. Fit of the θ_{rms}^{meas} as a function of the segment length for a single 3 GeV muon track.

those tracks longer than 5 meters we have used only this length, as using the whole track does not improve the results. For shorter tracks we used 10 segment lengths inside the interval [5 cm, 25 cm].

Assuming the distribution of RMS of scattering angles is Gaussian, it can be demonstrated that the momentum is distributed according to the following function:

$$\frac{1}{a_0\, p^2}\; exp\left(\frac{\frac{1}{p}-\frac{1}{a_1}}{a_2}\right)^2 \tag{4}$$

where a_1 gives an estimate of the momentum average.

Moreover, the momentum resolution Δp is estimated from the RMS of the distribution obtained after computing the different scattering angle RMS, given that $\frac{\Delta\theta^{rms}}{\theta^{rms}} \equiv \frac{\Delta p}{p}$. Figure 3 shows the distributions of $\frac{1}{p}$ together with the Gaussian fit, for two of the considered momenta.

The *classical* multiple scattering method, as described so far, obviously underestimates the particle momentum (see discussion in section 7). This is due to the fact that as the particle propagates in liquid Argon, it loses energy by means of ionization and therefore its momentum decreases. Since this method does not include any kind of compensation, the final result corresponds to

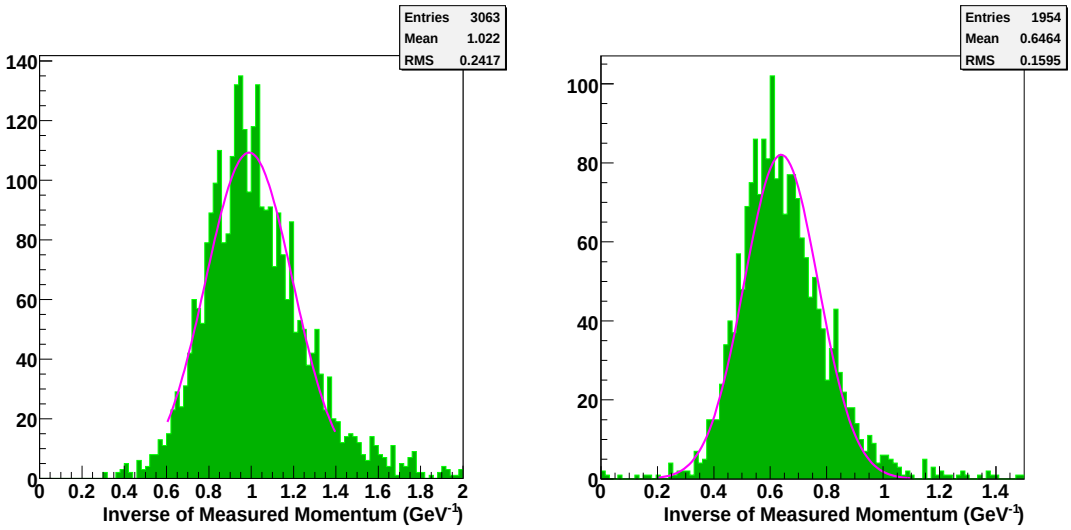

Fig. 3. Histograms of the inverse of the measured momentum for 1.5 and 2 GeV simulated muons.

an average reduced momentum and not to the momentum the particle had when it first entered the detector. The latter can be estimated performing an a posteriori correction since we know the track length and the mean energy deposition of a charged particle in liquid Argon. In the next section, we introduce a different approach, able to take into account energy losses along the muon track.

5 The Kalman Filter

The Kalman Filter [8] was originally proposed as an algorithm that deduces an optimum estimate of the past, present or future state of a dynamic system. It uses a time sequence of measurements of the system behaviour, information about its initial condition plus a statistical model that characterizes the system and the measurement errors. It provides a tool to separate random noises from signals in statistical processes.

Although originally proposed as a solution for problems in communication and signal control, the Kalman Filter has been used extensively in particle physics since it was first proposed as an alternative solution for track and vertex fitting and to estimate momenta [12]. Typically this technique has been used in association with data provided by magnetized detectors. When this filter is applied, the random noise introduced in the system by multiple scattering can be efficiently separated from the track bending due to the magnetic field. Therefore an improved momentum measurement can be obtained.

We now explore the possibility to apply the Kalman Filter algorithm in an homogeneous, non-magnetized environment (the one offered by the T600) in order to get a measurement of the momentum of charged particles. The parti-

cle momentum is extracted from the information provided by the distribution of angles arising from multiple Coulomb scattering process. The Kalman Filter helps to disentangle the noise introduced by the detector resolution. In parallel, it takes into account the energy loss along the track, thus improving the determination of its momentum.

The Kalman Filter must be applied to a dynamic set of discrete data, therefore the state vector of the system should be considered only for a discrete set of points, x_k. In our case, where an homogeneous fully-sensitive detector is considered, those points can be chosen anywhere along the track propagation direction. In practice, we split the track into a set of segments. The beginning and end points of those segments define a set of *planes* where we evaluate the state vector x_k.

The Kalman Filter is the optimal recursive estimator only in the case of a discrete *linear* dynamic system. This means that all equations describing the evolution of the state vector (covariance matrix, etc.) must be linear. In our particular problem, the dynamic system under study (a track) is described by the following equation:

$$x_k^- = F_{k-1}\, x_{k-1} + w_{k-1} \tag{5}$$

where F_{k-1} represents the *propagation of the state vector* from the plane k-1 to the plane k, and w_{k-1} represents the *noise* added to the propagation in liquid Argon, which is of random nature and therefore smears the state vector. As explained below, x_{k-1} and x_k^- refer to the *filtered* and *predicted* state vectors in planes *k-1* and *k*, respectively. Two are the sources of *noise* we must deal with: multiple scattering and energy loss.

Usually the state vector is not directly observed. For instance in our case the state vector contains the momentum of the particle, which is not measured. Instead, we measure the particle scattering angle. At this point, a new vector called *measurement vector* (m_k) must be introduced to connect the experimentally measured magnitudes with the state vector:

$$m_k = H_k\, x_k + \epsilon_k \tag{6}$$

where H_k is a matrix and ϵ_k represents the measurement noise or measurement errors. In general, m_k and x_k may have different dimensions.

The process (system) noise w_k is assumed to be unbiased and to have finite variance, being its covariance matrix Q_k. The measurement (detector) noise ϵ_k is assumed to be unbiased as well and to have finite variance.

$$\begin{aligned} E\{w_k\} &= 0 \qquad & \mathbf{Q}_k &\equiv cov\{w_k\} \\ E\{\epsilon_k\} &= 0 \qquad & \mathbf{V}_k &\equiv cov\{\epsilon_k\} \end{aligned} \tag{7}$$

If w_k and ϵ_k are Gaussian random variables, the Kalman Filter will be the optimal filter to the problem.

As shown in figure 4, the Kalman Filter proceeds through three conceptually different operations [b]:

- **Prediction.** Once the state vector in plane *k-1* is known, the prediction consists on estimating the state vector in a "future" plane k, assuming no noise. Then, x_k^{k-1} (we are using the convention $x_k^{k-1} = x_k^-$) will be the prediction of the state vector at plane k using the corresponding state vectors up to plane *k-1*.

$$x_k^- = F_{k-1}\, x_{k-1} \tag{8}$$

- **Filtering.** Known the predicted state vector in the plane k, the filtering consist in the determination of the "present" state vector taking into account the information provided by all past measurements (through the predicted state at plane k) and the present measurement. If there are no measurements at a given plane, filtering does not occur.

$$x_k = x_k^- + K_k(m_k - H_k\, x_k^-) \tag{9}$$

  where K is known as the *Kalman Gain* matrix and is related to the covariance of the state vector and the measurement noise.

- **Smoothing.** Once the filtering is applied to the plane *k+1*, the smooth process can be applied to estimate the state vector of a "past" plane k taking into account information up to plane *k+1*.

$$x_k^n = x_k + A_k(x_{k+1}^n - x_{k+1}^-) \tag{10}$$

  where A is called the *Smoothed Gain* matrix. Here, x_k^n refers to the final filtered state vector after smoothing in plane k.

The power of the method lies on the fact that all previous measurements are taken into account to predict the future dynamical behaviour of the system. Therefore, unlike the case of what we called the *classical* approach, where the set of reconstructed track segments is just a collection of unrelated measurements, the Kalman Filter does take correlations into account (in particular, energy losses are automatically included) and therefore we expect, a priori, an improved estimate of both the momentum and its resolution.

5.1 The Kalman Filter parameters

The application of the Kalman Filter technique requires the definition of a certain set of vectors and matrices. The values used throughout our calculation

[b] The complete set of formulae for the predicted, filtered and smoothed states can be found in [12].

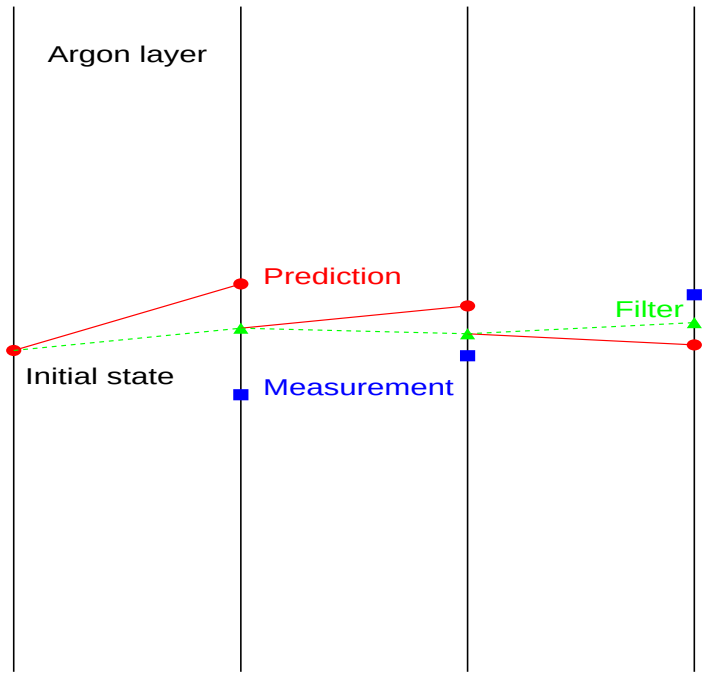

Fig. 4. Scheme of the Kalman Filter method. For a given initial state, the position is propagated linearly ("Prediction"). Then, the "Filtered" state is computed by comparing the "Measured" and the "Predicted" states. This procedure is repeated over all track layers. The "smoothing" is done by repeating the same process backwards.

are as follows:

1.- **State Vector:** To make the analysis, the track is split in segments of a certain length, and in each intersection we consider several magnitudes that will conform our state vector. In each of those segments the hits are fitted to a straight line. The parameters of the fit will define the state vector.

In the following, we will consider a three coordinate system, with our particle traveling in the z direction, and being x and y perpendicular to this direction. The state vector will be made of five variables:

- The inverse of the momentum of the particle. This magnitude is related with the angle between the current segment and the next one through the multiple scattering formula (see equation 1).
- The position of the particle in the plane (two components: x, y).
- The slope of the track in the plane (two components: $\frac{dx}{dz}, \frac{dy}{dz}$).

Hence,

$$\mathbf{x}_k = \begin{pmatrix} \frac{1}{p} \\ x \\ y \\ \frac{dx}{dz} \\ \frac{dy}{dz} \end{pmatrix} \tag{11}$$

2.- **Transportation Matrix:** The propagation matrix performs a straight line extrapolation and does not change the slopes, that is, assumes no interaction. The inverse of the momentum is propagated by subtracting from the momentum the energy lost along the segment length. This energy loss can be directly computed from the charge deposited in the wires by the particle along its path.

$$\mathbf{F}_k = \begin{pmatrix} \frac{1}{1-\frac{E_{lost}}{p}} & 0 & 0 & 0 & 0 \\ 0 & 1 & 0 & \Delta z & 0 \\ 0 & 0 & 1 & 0 & \Delta z \\ 0 & 0 & 0 & 1 & 0 \\ 0 & 0 & 0 & 0 & 1 \end{pmatrix} \tag{12}$$

3.- **Measurement Vector and Matrix:** The measurement vector is similar to the state vector. The only difference is in the first row, as momentum can not be measured directly. The measured magnitude is instead the angle difference between the incoming and outgoing trajectories, that is related with the momentum through equation 1. This difference is taken into account in the measurement matrix, and hence, measurement vector and measurement matrix are given by:

$$\mathbf{m}_k = \begin{pmatrix} \theta_0 \\ x \\ y \\ \frac{dx}{dz} \\ \frac{dy}{dz} \end{pmatrix}, \quad \mathbf{H}_k = \begin{pmatrix} C & & & & \\ & 1 & & & \\ & & 1 & & \\ & & & 1 & \\ & & & & 1 \end{pmatrix} \tag{13}$$

Where C is the multiple scattering constant that multiplies $\frac{1}{p}$ in equation 1.

4.- **Covariance Matrices:** The last ingredient for the method is the choice of the covariance matrices. The covariance matrix for the system noise has

been taken from reference [13] where the authors derive, in a simple and intuitive way, the track parameter covariance matrix due to multiple scattering. They obtain all the matrix elements for two experimentally relevant track parameterizations, being the first of them the one we are using: x and y slopes and intercepts.

In the covariance matrix for the detector noise, we have considered no correlations between the components of the state vector, and hence the matrix is diagonal. The value for each point is just the measurement error. This amounts to 400 μm.

6 Test of the Kalman Filter method on a Monte-Carlo Sample

To assess the correctness of the choices made in the previous section in order to build a Kalman Filter algorithm suitable to be applied to an homogeneous non-magnetized detector, we have simulated sets of 1000 Monte-Carlo muons for each of the following momenta: 0.25, 0.5, 1.0, 1.5, 2.0 and 3.0 GeV.

As explained in section 5, an initial state must be supplied for the method to work. It can be thought, a priori, that the input guess for the initial momentum is an important choice that may influence the final value of the momentum measurement. In practice this is avoided by giving a big enough error to the momentum in the first plane, such that its value becomes irrelevant. This has been tested by carrying out a Kalman Filter with a random initial state as input. The obtained momentum, close to the real one, was used as input for a second Kalman Filter. The final momentum does not differ significantly from the value used as input.

The only important choice for the method is the segment length to be used in the analysis. This must be as short as possible in order to guarantee a large enough number of points, but at the same time segments must be long enough in order to allow multiple scattering effects to emerge over the detector noise. Hence a compromise must be reached.

A priori, the most ambitious idea would be to consider just single hits, as in this way all the information is taken into account and no average is done. But when the segment length is too short, the noise in the measurements is too high, hiding multiple scattering effects. Therefore the momentum can not be properly estimated. We have seen that to optimize our results it is advisable to use three different segment lengths for each track. For all tracks, we have considered segment lengths of 10, 12.5 and 15 cm. The final momentum value is obtained by averaging the momentum computed for each of the selected segment lengths.

Figure 5 shows the calculated momentum distribution for two Monte-Carlo momenta. Each histogram entry corresponds to a reconstructed muon track. A Gaussian has been over-imposed to each histogram. The Gaussian curve fits

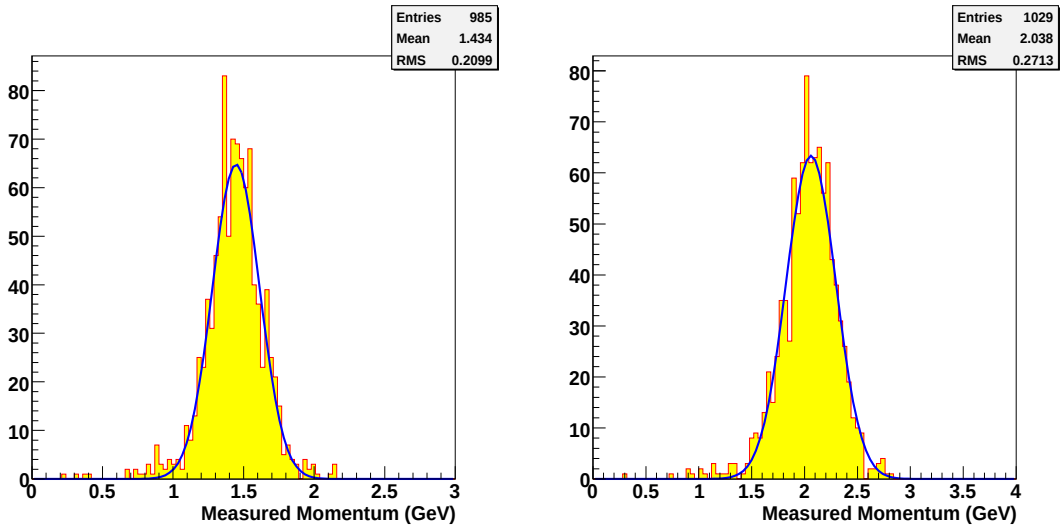

Fig. 5. Momentum distributions as given by the Kalman Filter for simulated muons of 1.5 and 2.0 GeV.

very well the outline of the histogram. This clearly proves that the Kalman Filter technique allows to have a precise measurement of the muon momentum on a track by track basis.

We note here an intrinsic limitation of the Kalman Filter method. It is well known that deviations from the original trajectory, due to multiple scattering, become smaller as momentum increases. Detector noise starts playing a more important role and it becomes necessary to go to longer segment lengths to observe multiple scattering effects. Therefore for much higher momenta, a different set of segment lengths should be used. In the limit of very high momentum, O(10 GeV), when multiple scattering effects are small, the Kalman Filter procedure is not able to give a proper estimation of the particle momentum.

7 Comparison of the performance of the *classical* and Kalman Filter approaches on a Monte-Carlo Sample

We have discussed separately two algorithms aiming at measuring the momentum of partially contained tracks. To summarize the most relevant points, we now compare the performance of both methods. The comparison is based on Monte-Carlo data. Figures 6 and 7 show the calibration curve and the resolutions obtained using the two methods.

In figure 6, the solid line shows the case where $P_{measured} = P_{Monte-Carlo}$. The points from the *classical* analysis are clearly below the line because of the energy lost by the muon along its path. For this approach, the error bars correspond to the RMS of each single distribution (similar to those shown in figure 3).

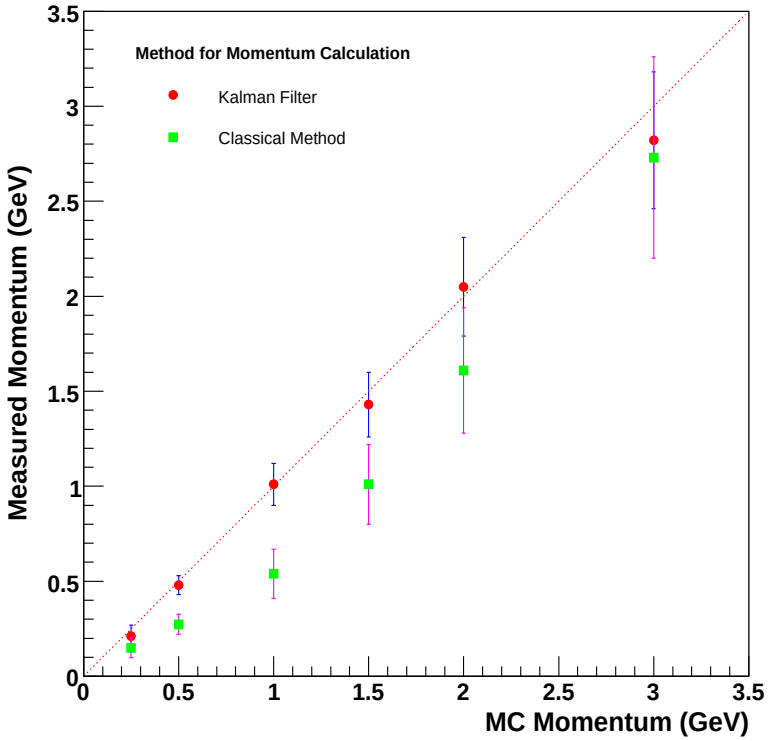

Fig. 6. Comparison between the calibration curves for *classical* and Kalman Filter methods.

The Kalman Filter gives a much better estimation, since it takes into account energy losses. For this algorithm, the error is taken as the RMS of the Gaussian fit to the individual momentum distributions similar to those of figure 5. Within one standard deviation, the Kalman Filter does not underestimate muon momentum. Therefore, contrary to the *classical* method where we calculate the mean momentum along the track, with the Kalman Filter the momentum at each plane can be calculated, and in particular, we can get a measurement of the most relevant magnitude, namely: the momentum at the initial plane.

Figure 7 shows the momentum resolution. For the *classical* approach it is on the range 25–20 %. There is an increase of the resolution at the edges: for small momenta, where the range of lengths and the number of segments is small, and for high momenta, where the effect of the multiple scattering decreases.

With the Kalman Filter technique, the resolutions are around 10% for the whole range of studied momenta, except at 250 MeV where the resolution is close to 25%. This increase is easily understandable given the short track lengths involved. A 250 MeV muon has a typical length of less than 1 meter. The amount of planes in which it can be split is small. Hence the method does not have enough information to provide an accurate measurement. In spite of that, 250 MeV events are typically fully contained and measured by calorimetry with a very good resolution. The inclusion of this energy in the

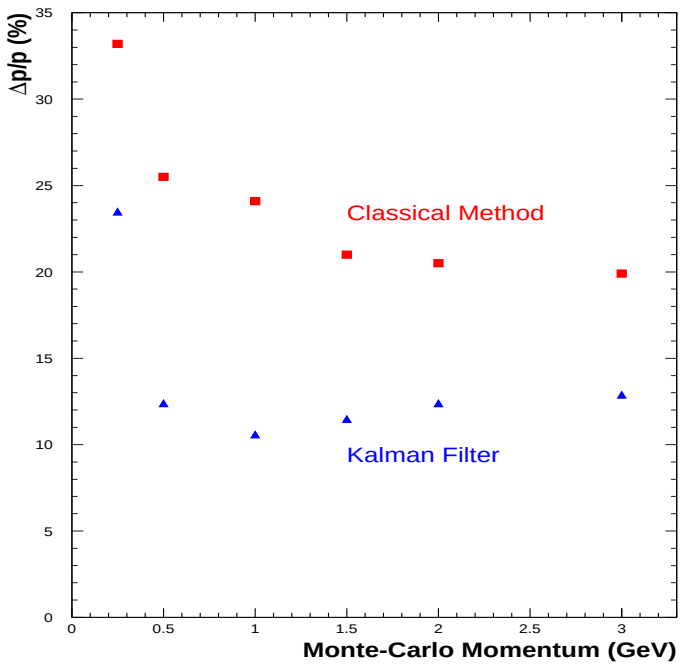

Fig. 7. Comparison between the resolutions for *classical* and Kalman Filter methods.

analysis was motivated by the aim to find the limits of the method.

We have also studied how the momentum resolution gets affected as the recorded track length gets shorter. This is specially important for the case of several GeV muons. Figure 8 shows, for the range of considered momenta, the expected resolutions when recorded tracks are 50, 100, 150, 200 and 250 cm long. We observed that, for all lengths, the momentum scale is not underestimated on average. Resolutions keep themselves in the interval 20–25%. Only for the shortest considered tracks (50 cm), the resolution worsens up to 30%. We conclude that, for tracks of a few GeV, the Kalman Filter allows to have a reasonable estimate of the charged particle momenta even if the recorded tracks are no longer than a meter.

In conclusion, with the *classical* approach we expect resolutions in the range 25–20 % and a underestimation of the momentum value. The results obtained with the Kalman Filter do not underestimate momentum and improve the resolution by almost a factor two. In addition, we notice that both methods exhibit a similar behavior at low energies, with an increase in the error with respect to the almost constant one for the rest of energies. This behavior appears at 500 MeV for the classical method and only at 250 MeV for the Kalman Filter. In both cases the error increase has to do with the length of the tracks and the small amount of available segments.

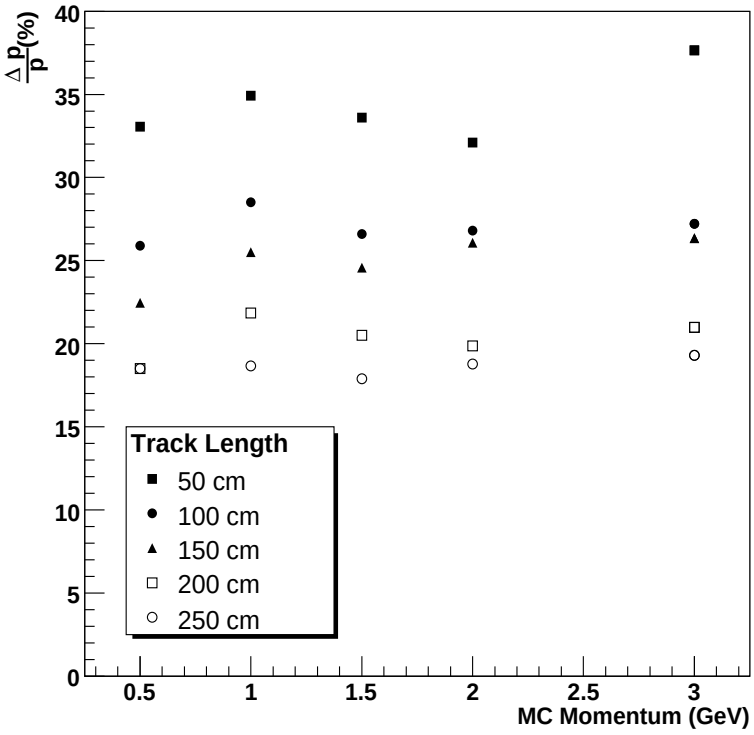

Fig. 8. Kalman Filter algorithm: Monte-Carlo momentum resolution as a function of the recorded track length.

8 Kalman Filter application to a set of stopping atmospheric muons

So far, we have just relied on Monte-Carlo data to show that the Kalman Filter is an optimal tool to estimate the momentum of partially contained tracks. We now try to assess the goodness of this algorithm by applying it to real data. The sample we take as reference corresponds to a set of stopping atmospheric muons collected on the summer of 2001 during a T600 technical run on surface. The initial set contains the 2690 events used in [5]. We impose the condition that, in the collection view, muons should have at least 60 hits and a minimum track length of 50 cm. These requirements leave us with a final sample of 1009 muons.

Given the characteristics of the selected muons, the range of considered momenta spans from about 200 MeV up to 800 MeV (being the mean value 400 MeV). For higher momenta, the sample of recorded muons is not statistically significant. The Monte-Carlo tells us that the Kalman Filter performance for the lower momentum range is not as good as the one expected for muons above 1 GeV. However a demonstration that the method performs reasonably well in the low momentum range, will give us confidence on the fact that the algorithm can be also applied at higher momenta.

The selected data have been reconstructed following the procedure outlined

in Section 3. Being fully contained, the momentum of those muons can be very accurately measured using a calorimetric approach. When computing momentum by means of calorimetry, recombination effects should be taken into account. Equation 14 relates measured and deposited charges, being R the electron recombination factor in liquid Argon:

$$Q_{meas} = R \cdot Q_{dep} \cdot e^{\frac{t-t_0}{\tau}} \tag{14}$$

We take from [2] the value $R = 0.71$. τ stands for the drift mean life of the electrons and its value is taken from [3]. The error associated to τ is propagated to the momentum measured by calorimetry. It amounts to less than five per cent.

In our approach we consider the momentum measured by calorimetry, p_{cal}, as the *true* momentum value. On a track by track basis, we compare the momentum obtained with the Kalman Filter, p_{kf}, to p_{cal}. The results are shown in figures 9 and 10.

We plot the profile of the analyzed data set in figure 9. It shows that, on average, our measurements tend to cluster around the solid line, which depicts the ideal condition where $p_{kf} = p_{cal}$. In the high momentum region, the decrease of statistics results in bigger fluctuations around the central line. From the plot we infer that the relationship among the two performed measurements is clearly linear, thus showing that the Kalman Filter gives a good measurement of real data momentum.

We also plot the dispersion of the Kalman Filter measurements with respect to p_{cal} in figure 10. For each of the six momentum bins into which we group the data, the mean dispersion is very close to zero. The error bars correspond to the RMS of each individual distribution. For the lowest momenta, the error is around 20%. As the momentum increases, the error bar diminishes reaching a minimum value of about 12%. These results are in very good agreement with the resolutions obtained, for the low momentum range, in our Monte-Carlo simulation (see figure 7). In view of these results, we conclude that real data confirm the fact that the Kalman Filter algorithm, when combined with multiple Coulomb scattering information, is an optimal method to obtain an accurate measurement of partially contained track momenta.

9 Conclusions

We have addressed the problem of measuring the momentum of partially contained charged particles recorded with the 600 ton ICARUS detector. This is a fundamental issue in our effort to study very precisely atmospheric neutrinos.

We have analyzed the performance of two independent approaches:

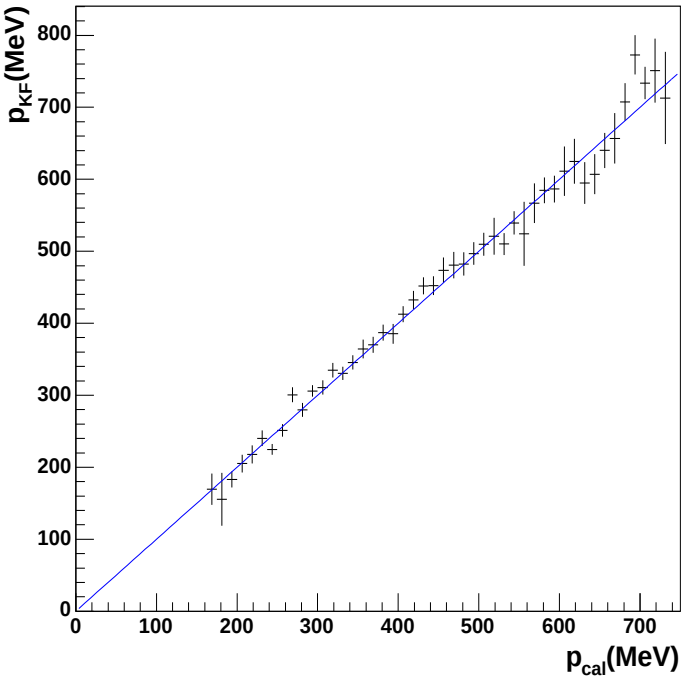

Fig. 9. Profile plot of the correlation between the momentum measured by calorimetry p_{cal} and the one obtained by means of a Kalman Filter, p_{kf}.

- The one referred to as *classical* extracts the momentum from the distribution of scattering angles measured along the particle trajectory. We have proposed an algorithm that avoids defining an optimized segment length for the computation of the scattering angles.
- The second method is based on a Kalman Filter. We have explored, for the first time, the possibility to apply this algorithm in an homogeneous, non-magnetized environment. This method takes all measurements into account to predict the future dynamical behaviour of the considered system. Therefore, unlike the *classical* approach, where the set of reconstructed track segments is just a collection of unrelated measurements, the Kalman Filter does take correlations into account (in particular, energy losses are automatically included).

With the *classical* method, the momentum is underestimated (since energy losses are not considered). The expected resolutions lie around 25% for a range of momenta ranging from 250 MeV up to 3 GeV. With the Kalman Filter, momentum is not underestimated and the expected resolutions improve by a factor two those obtained with the *classical* method. We have also observed that, for tracks with momentum in the vicinity of 1 GeV or higher, the Kalman Filter provides a reasonable momentum measurement, even in the case the recorded tracks are around one meter long.

To assess the goodness of the Kalman Filter approach, we have used a set of real data composed of atmospheric muons that stop inside the detector. The

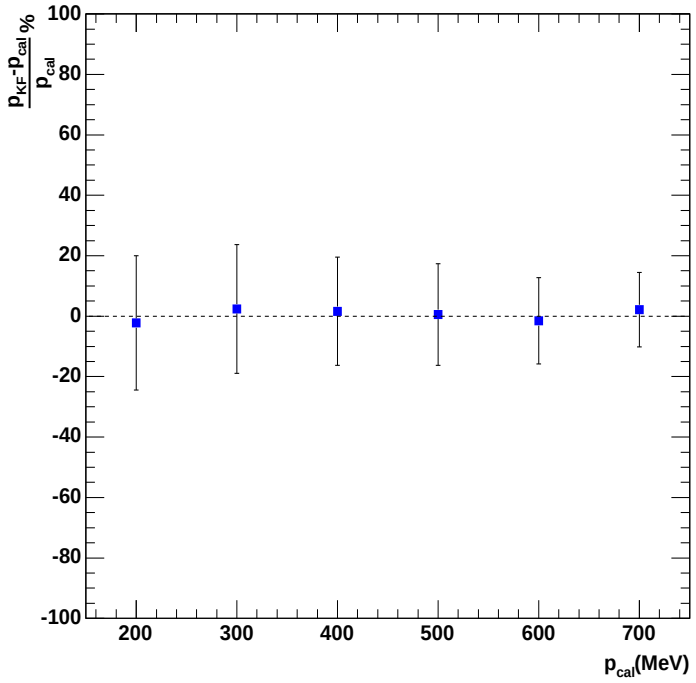

Fig. 10. Dispersion of the Kalman Filter measurements with respect to the momentum measured by calorimetry, p_{cal}. The filled squares represent the mean value of the dispersion distribution. The error bars correspond to the RMS.

momentum of those muons is very precisely measured by calorimetry. The momentum estimation provided by the Kalman Filter shows a very good agreement with calorimetric measurements, proving the validity of the method. We therefore conclude that the Kalman Filter approach is an excellent tool to get precise kinematics information of the set of partially contained atmospheric neutrino events that we expect to record at the Gran Sasso underground laboratory.

10 Acknowledgments

We would like to warmly thank the many technical collaborators that contributed to the construction of the detector and to its operation. We are glad of the financial and technical support of our funding agencies and in particular of the Istituto Nazionale di Fisica Nucleare (INFN), of ETH Zürich and of the Fonds National Suisse de la Recherche Scientifique, Switzerland. This work has been supported by the CICYT Grant FPA2002-01835. The Polish groups acknowledge the support of the State Committee for Scientific Research in Poland, 105,160,620,621/E-344,E-340, E-77,E-78/SPS/ICARUS/P-03/DZ211-214/2003-2005 and 1P03B 041 30; the INFN, FAI program; the EU Commission, TA-DUSL-P2004-08-LNGS.

References

[1] S. Amerio *et al.* [ICARUS Collaboration], Nucl. Instrum. Meth. A **527**, 329 (2004).

[2] S. Amoruso *et al.* [ICARUS Collaboration], Nucl. Instrum. Meth. A **523**, 275 (2004).

[3] S. Amoruso *et al.* [ICARUS Collaboration], Nucl. Instrum. Meth. A **516**, 68 (2004).

[4] M. Antonello *et al.* [ICARUS Collaboration], Nucl. Instrum. Meth. A **516**, 348 (2004).

[5] S. Amoruso *et al.* [ICARUS Collaboration], Eur. Phys. J. C **33**, 233 (2004).

[6] F. Arneodo *et al.* [ICARUS Collaboration], Nucl. Instrum. Meth. A **508**, 287 (2003) [Erratum-ibid. A **516**, 610 (2004)].

[7] F. Arneodo *et al.* [ICARUS Collaboration], LNGS P28/01, LNGS-EXP 13/89 add. 1/01; arXiv:hep-ex/0103008.

[8] R. E. Kalman, Trans. ASME, J. Bas. Eng. **82D** (1960).

[9] P. Cennini *et al.* [ICARUS Collaboration], *Nucl. Instr. and Meth.* **A 432**, 240 (1999).

[10] G. Battistoni, A. Ferrari, T. Montaruli and P. Sala, Astr. Part. Phys. **19**, 269 (2003). See `http://www.fluka.org/` for further details.

[11] S. Eidelman *et al.* [Particle Data Group], Phys. Lett. B **592**, 1 (2004).

[12] R. Fruhwirth, Nucl. Instrum. Meth. A **262** 444 (1987).

[13] E. J. Wolin and L. L. Ho, Nucl. Instrum. Meth. A **329** 493 (1993).